

Integration of Muscle Pre-tension and Activation to Evaluate Neck Muscle Strain Injury Risk during Simulated Rear Impacts Using a Finite Element Neck Model

Matheus A. Correia, Stewart D. McLachlin, Duane S. Cronin
Department of Mechanical and Mechatronics Engineering, University of Waterloo

ABSTRACT – Prevention of rear-impact neck injuries remains challenging for safety designers due to a lack of understanding of the tissue-level response and injury risk. Soft tissue injuries have been inferred from clinical, cadaveric, and numerical studies; however, there is a paucity of data for neck muscle injury, commonly reported as muscle pain. The goal of this study was to investigate the effect of muscle pre-tension and activation on muscle strain and injury risk resulting from low-severity rear impacts using a detailed finite element head and neck model (HNM).

The HNM was extracted from the GHBMCA average stature male model and re-postured to match a volunteer study, with measured T1 kinematics applied as boundary conditions to the HNM. Three cases were simulated for three impact severities: the baseline re-postured HNM, the HNM including muscle pre-tension, and the HNM with muscle pre-tension and muscle activation. The head kinematics, vertebral kinematics, muscle strains, and three neck injury criteria were calculated to assess injury risk.

The kinematic response of the neck model demonstrated an S-shaped pattern, followed by extension in the rear impact cases. The maximum kinetics, kinematics, and muscle strains occurred later in the impact during the extension phase. The distribution and magnitude of muscle strain depended on muscle pre-tension and activation, and the largest predicted strains occurred at locations associated with muscle injury reported in the literature. The HNM with muscle pre-tension and muscle activation provides a tool to assess rear impact response and could inform injury mitigation strategies in the future.

KEYWORDS – Whiplash, muscle injury, rear impact, finite elements, human body model, muscle activation.

INTRODUCTION

A recent study investigating vehicle crash data from 2001 to 2021 found that 25% of the cases corresponded to rear impacts (Swain and Larue 2024). For these rear impacts, 35% of the incidents required medical treatment and 14% required hospitalization (Swain and Larue 2024). Whiplash-associated disorders (WADs) are of special interest in rear impacts due to the high economic cost involved, approximately \$2.7 billion annually in the United States (Hayashi et al. 2023). Although extensive research has been undertaken to investigate the cause and risk of such injuries in automotive impacts (Corrales and Cronin 2021; Putra and Thomson 2022; Yoganandan, Harinathan, and Vedantam 2024), a full

explanation of the locations and tissues injured, has not yet been established.

Previous sled test studies with both post-mortem human subjects (PMHS) and living human volunteers have shown that during rear impacts, the neck, initially considered to be in a neutral posture (lordotic curvature), quickly transitions into upper cervical spine flexion and lower cervical spine extension (S-shape), followed by the entire neck rotating into extension (C-shape) (Stemper and Corner 2016). Some studies have proposed that injury occurs during the S-shape phase (Stemper and Corner 2016).

The soft tissues of the neck are frequently discussed as potential sources of pain (Hallgren and Rowan 2021; Stemper and Corner 2016; Vasavada, Brault, and Siegmund 2007). The facet joints, spinal ligaments, intervertebral discs, vertebral arteries,

Address correspondence to: Matheus Augusto Correia,
University of Waterloo, 200 University Avenue West Waterloo,
ON, Canada N2L 3G1
Electronic mail: matheus.correia@uwaterloo.ca

dorsal root ganglia, and neck muscles were identified in previous studies as possible locations of injury in WAD (Li et al. 2019). Cadaveric, surgical, magnetic resonance imaging and animal studies have correlated damage to the ligaments, intervertebral disc, and facet joint with WADs (Li et al. 2019). However, few investigations of injury in the neck muscles exist even though electromyographic measurements and computational studies indicated the possibility of injury in this tissue due to active contraction against a stretching motion during impacts (Brault, Siegmund, and Wheeler 2000; Vasavada et al. 2007). In addition, identifying soft tissue injury thresholds using anthropometric testing devices (ATD) and PMHS has proved challenging as there are large differences between these surrogates and the *in vivo* tissue behavior.

One possible solution is the use of computational human body models (HBMs) with sufficient detail to assess tissue-level responses. The head and neck of the Global Human Body Model Consortium (GHBMC) model for a 50th percentile young male (M50-O version 5.1) is a good candidate for investigating neck muscle strains during impacts (Correia et al. 2023). The M50 (Figure 1) includes detailed representations of the muscles, skin, ligaments, intervertebral discs, vertebrae, and head. One-dimensional Hill-type elements represent the active muscle contraction and three-dimensional hexahedral elements with visco-hyperelastic response represent the passive muscle tissue response.

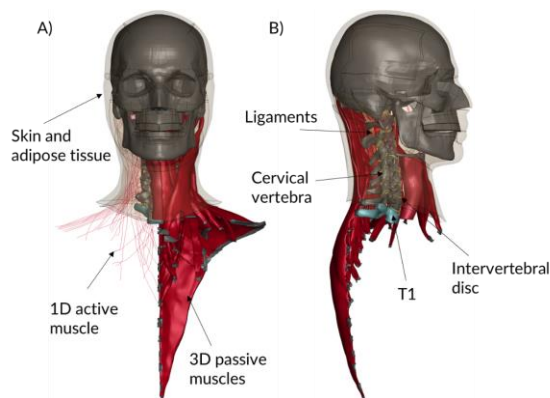


Figure 1: A) Frontal view of the M50 head and neck model with the right three-dimensional passive muscle elements hidden. B) Lateral view of the M50 head and neck model with all the right muscle elements hidden.

Recent studies have enhanced the GHBMC head and neck model to improve the muscle tissue response in impact scenarios (Corrales, Correia, and Cronin 2021; Gierczycka, Rycman, and Cronin 2021;

Hadagali and Cronin 2023). A novel enhancement to the GHBMC neck musculature was the constrained beam in solid (CBS) methodology, which coupled the one-dimensional Hill-type active elements with the three-dimensional solid passive muscle tissue elements (Corrales et al. 2021; Correia et al. 2023). The CBS method enabled improved prediction of strain in the muscles and no longer required the unphysical attachment elements between the Hill active elements and the vertebra. The CBS method improved the muscle implementation to represent biofidelic muscle strains for the first time (Corrales et al. 2021; Correia et al. 2023). Another study showed that the model presented good correspondence to multidirectional human volunteer impact studies for a physiologically based closed-loop controller based on the vestibulocollic reflex (VCR) and cervicocollic reflex (CCR) mechanisms of the neck (Correia, McLachlin, and Cronin 2021). The VCR modulates muscle activation by structures in the inner ear that measure the head kinematics, and the CCR modulates muscle activation by specialized cells that measure muscle stretch. The closed-loop controller used proportional-derivative (PD) controllers, as they agree with the equilibrium-point hypothesis (Jagodnik et al. 2015) and were able to represent reflex mechanisms in previous studies (Putra et al. 2021). The closed-loop activation used the head center of gravity rotation in the X, Y, and Z axes as input of the PD controllers representing the VCR and the 1D Hill-type element stretches as input to the PD controller representing the CCR.

In a recent HBM study (Correia et al. 2023), a muscle pre-tension method was proposed for initiating stresses present in the muscle due to *in situ* pre-stretch, before the impact. The pre-tension stress in the model was obtained by deforming the muscle from the slack length (relaxed and non-deformed length) to the model *in situ* length (length in an upright neutral posture). Based on estimations from cadaveric measurements, the flexor slack lengths were 8% shorter than the *in situ* muscle lengths, while the extensor slack lengths were 3% shorter than the *in situ* length (Correia et al. 2023). Implementing pre-tension improved the upper cervical spine kinematics, better representing the S-shape reported in the literature for volunteer impacts.

Ideally, the validation of simulated active muscles in HBMs should be achieved by measuring muscle forces *in vivo*, but this remains a large challenge to ethically and safely conduct such experiments in humans (Wakeling, Febrer-Nafria, and De Groot 2023). Alternatively, human volunteer experimental data reporting vertebral kinematics could help to

assess the neck muscle implementation response. Sato et al. (Sato et al. 2014) conducted a study to measure the neck dynamics of male and female volunteers in low-severity rear impacts. For one of the three rear impact pulses analyzed by Sato et al. (Sato et al. 2014), the individual vertebral kinematics were recorded with cineradiography during 4g rear impacts and, therefore, could be used for comparison to a neck model at the vertebral level. In addition, a related work (Sato et al. 2016) measured the average posture of males seated in a similar seat from Sato *et al.* (Sato et al. 2014) Posture has been shown to be an important factor in neck response during impacts (John, Saravana Kumar, and Yoganandan 2019). It is important to note that even though studies with volunteers are better suited for the analysis of models with muscle activation, past cadaveric studies also presented vertebral kinematics for rear impacts, like Deng et al. 2000 (Deng et al. 2000) with higher severities (>6g) and Stemper et al. 2004 (Stemper, Yoganandan, and Pintar 2004) for lower severities (4g). In addition, cadaveric studies have also been used to correlate intervertebral rotations to potential soft tissue injury risk (Bumberger, Acar, and Bouazza-Marouf 2020).

The assessment of neck injury risk in ATDs and models is achieved using injury risk criteria. Over the years, different criteria have been proposed (Li et al. 2019; Schmitt et al. 2014): the Neck Injury Criterion (NIC), based on pressure gradients relation to the spinal cord damage, is calculated using accelerations and velocities of C1 and T1 vertebrae; the intervertebral Neck Injury Criterion (IV-NIC), is defined as the intervertebral motion divided by the physiological range of motion; the Nij injury criterion, based on a combination of the axial force and the bending moment in frontal impacts; the N_{km} , based on a combination of the axial force and the bending moment in rear impacts; the Lower-Neck Load Index (LNL), based on the loads at the T1 vertebra related to facet joint injury; and the Neck Displacement Criterion (NDC), based on graphs of the angular velocity and displacement of the head relative to the T1 vertebra.

An alternative approach to evaluating injury risk in detailed HBMs is a tissue-level assessment (DeWit and Cronin 2012) directly comparing the values of muscle strains from the model and the experimental data on muscle tears or pain. The range of reported deformations over which muscles rupture, observed in experiments with excised specimens, is relatively large. Experimental data reported engineering strain at failure ranging from 0.23 to 0.42 (Hasselmann et al. 1995) for active stretch, and failure Green strain

between 0.50 and 0.62 when no activation was present (Best et al. 1995; Morrow et al. 2010).

In the present study, the GHBMCM50-O head and neck model was used to assess how the combination of muscle activation and pre-tension alters the distribution of 3D muscle strains in rear impacts. The strains were compared with experimental data on muscle tissue failure, and the head and neck response with traditional neck injury criteria, to assess the relation of muscle strain to injury risk.

METHODS

The head and neck regions were extracted from the GHBMCM50-O v5.1 (M50) model, representing a 50th percentile male. The head and neck posture was changed (Correia et al. 2023) to match the volunteers sitting in a sled in rear impact experiments (Sato et al. 2016). The muscles of the model were updated by implementing the CBS methodology, and the CBS was integrated with muscle pre-tension (Correia et al. 2023) and open-loop active muscle control (Correia et al. 2021).

Rear impacts were simulated by applying measured T1 kinematics from 4g rear impact experiments with volunteers from the literature (Sato et al. 2014). The boundary conditions of higher severity impacts (7g and 10g (Deng et al. 2000)) from PMHS testing were also simulated.

To assess the effects of the different muscle implementations, the rear impact scenarios were simulated for three different versions of the model: the M50 extracted from the full body model; the M50 model with muscle pre-tension, but no muscle activation (M50_p); and the M50 model with pre-tension and closed-loop muscle activation (M50_{pc}). Finally, the head kinematics, vertebral kinematics, muscle strains, and three neck injury criteria were calculated to quantify response and injury risk in the simulated scenarios.

Neck muscle pre-tension implemented in the M50_p and M50_{pc} head and neck model

The neck muscle pre-tension was defined in this work as the muscle stretch corresponding to a neutral, relaxed posture before the simulated impact or muscle activation. The objective of the muscle pre-tension was to better replicate stresses present in the muscle tissue *in vivo*. The pre-tension stress in the model was obtained by deforming the muscle from the shorter muscle slack length (muscle length with no stresses) to the longer *in situ* length (muscle length in a neutral position prior to the impact simulation).

The simulations were carried out in 32 cores using a single precision commercial FE solver (LS-DYNA, R.9.3.0). The stress initialization for muscle pre-tension was conducted in two steps as reported in a recent study (Correia et al. 2023). First, a dynamic relaxation simulation was conducted to obtain the deformations of the muscle from the slack length to the *in situ* length. Second, an explicit simulation was run for 200 ms with T1 fixed and gravity loading to allow the passive pre-stretched musculature to reach a quasi-equilibrium state. The two steps and the subsequent impact were conducted directly one after the other in the same simulation. The 200 ms stabilization period was run for the three models and led to initial strains (pre-stretch) in the muscles. The postures of the three models were not the same after the stabilization.

Closed-loop neck muscle activation implemented in the M50_{PC} head and neck model

The closed-loop muscle activation was based on a controller scheme from a previous publication

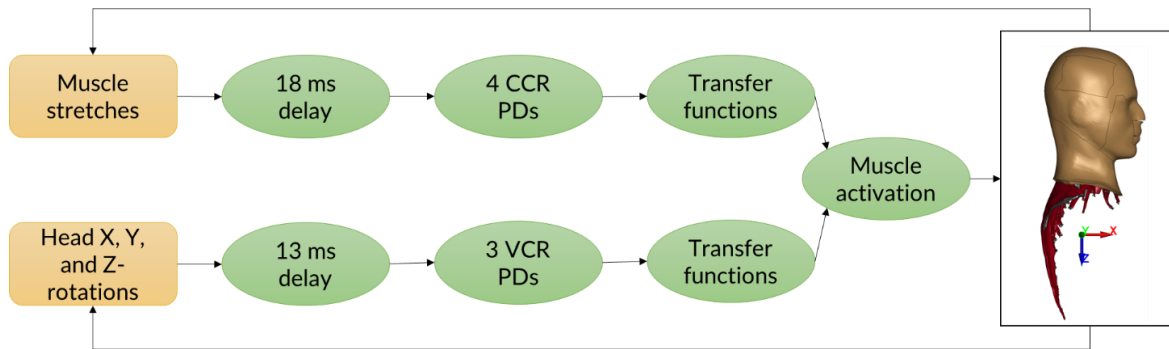


Figure 2: Closed-loop controller schematic of the muscle activation. The head rotation and muscle stretches are the inputs of the controller. The CCR and VCR delays for each of the four muscles were based on experimental data. The delays are applied to the inputs using PD controllers. The outputs of the PDs are combined and transformed into an activation level to be applied to the muscle through transfer functions.

(Correia et al. 2021) based on the physiological reflex mechanisms of the neck (Figure 2).

For the current study, the controllers were updated with a time delay of 13 ms for the VCR and 18 ms for the CCR, based on experimental data (Happee et al. 2017). The 13 ms delay was the time needed for the signal generated by the head rotation to affect muscle activation. The 18 ms delay was the time needed for the signal generated by the muscle stretch to affect the muscle activation. The input of the CCR was simplified as the changes in length between the origin and insertion point of the Hill-type beam elements at the medial portion of the trapezius and the sternocleidomastoid muscles (Figure 3). In addition, each one of the four muscle groups (right extensors, left extensors, left flexors, and right flexors) was controlled separately (Correia et al. 2021).

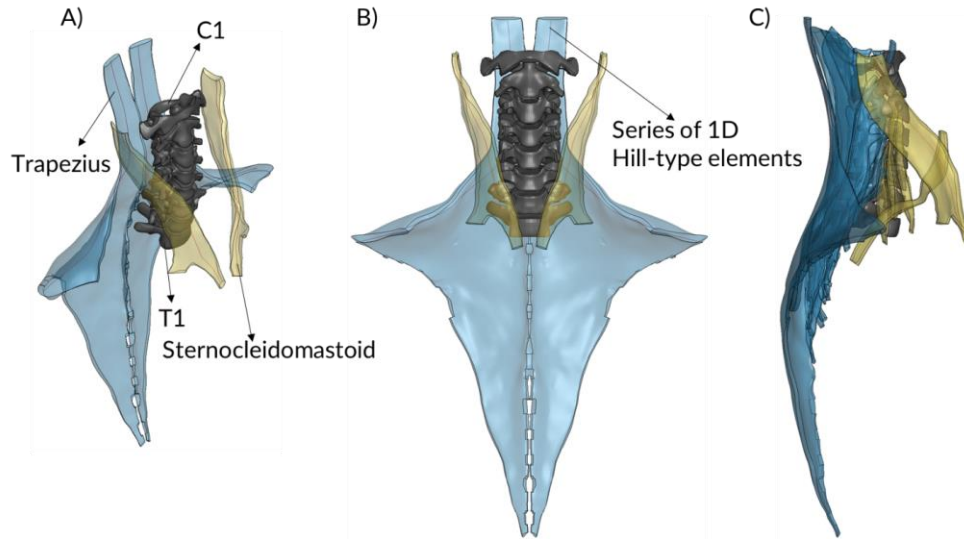


Figure 3: A) Isometric view of the sternocleidomastoid, trapezius, and cervical spine. B) Frontal view of the series of 1D Hill-type elements (red lines) used as input for the closed-loop controller. C) Lateral view of the flexors (red) and extensors (blue).

The elements for the CCR input were selected from the muscles presenting the highest force and deformation after observing frontal and rear impact simulations without muscle activation. Due to the muscle pre-tension, the controller parameters had to be optimized for this new scenario. A Python code was implemented to optimize the proportional and derivative gains of the PD controllers. The optimization fitted the activation curves of the closed-loop controller to the co-contraction activation curves of an open-loop controller (Correia et al. 2021). The optimization used the head rotation and muscle stretches from the open-loop controller simulation as the input signals. For the VCR, the proportional gain obtained through this methodology was 0.44 and the derivative gain was equal to 14.9. For the CCR, the proportional gain was 0.063 and the derivative gain was equal to 0 for the extensors, and 0.28 and 4.5, respectively, for the flexors. The VCR maintained an activation ratio of 1:5 between the extensors and flexors to maintain the cocontraction ratio from a previous study (Correia et al. 2021). The VCR gains were positive for the antagonistic muscle groups, relative to the head rotation, and negative for the agonist muscles. The CCR gains were positive for lengthening and zero for shortening of the muscles relative to the resting length. It is important to note that, during the simulation, Massively Parallel Processing (MPP) decomposition was used so the 3D muscles and 1D Hill elements calculations occurred in the same core. The MPP decomposition was necessary to ensure numerical consistency among the two muscle parts.

Rear impact simulation

Low-acceleration rear impact simulations were run using three different models: M50, M50_p, and M50_{pc} to calculate the muscle deformations during the impact. The average X-displacement, Y-rotation, and Z-displacement of the T1 vertebra of the experiment with 4 male volunteers from Sato *et al.* 2014 (Sato et al. 2014) were applied to the T1 vertebra of the models. The X-rotation, Z-rotation, and Y-translation of T1 were free to move. The muscle, skin, and flesh ends were constrained to T1 to represent the boundary condition of the torso (Appendix Figure A1). These boundary conditions represented a rear impact with a peak acceleration of approximately 4g and were selected as the recorded vertebral kinematics were available for comparison with the model results. The applied X-displacement was obtained by double integrating the X-acceleration presented in the literature. Also, two additional 7g and 10g impacts were simulated with the M50_{pc} for a subsequent analysis of the effect of the severity on the possibility of injury. The M50_{pc} was selected for the severity analysis because it presented the highest muscle strains and therefore the most injurious scenario. For these high-severity impacts, the X-acceleration, Y-rotation, and Z-acceleration from Deng et al. 2000 (Deng et al. 2000) study with PMHS were applied to the T1 of the M50_{pc}.

The resultant head and vertebral kinematics of the simulations were extracted and compared to the experiments to verify the simulations. The 95th percentile of the maximum principal strains (MPS)

from the muscles were extracted and compared with muscle failure data. The strain time histories and strain distribution were inspected for the 3D passive elements in all simulations. The highest spurious values were associated with the muscle-tendon interface, and the 95th percentile criterion consistently reported the relevant muscle strains occurring in the muscle while excluding the high strains at the tendon-muscle interface. (Figure A4, Appendix). Furthermore, the Neck Injury Criterion (NIC), the N_{km} injury criterion, and the intervertebral Neck Injury Criterion (IV-NIC) were calculated for the simulations to compare the capabilities of these criteria to identify possible muscle injury. Although N_{km} is usually measured at the occiput (close to C0/C1), this criterion was used in all vertebral joints for comparison to the IV-NIC. The forces and moments at the cervical spine required to calculate the injury criteria were obtained following a similar approach to the cross-section method used by Johnson *et al.* (Johnson, Koya, and Gayzik 2020). No filtering was applied to the force and moment histories, and the data was sampled at 200 Hz. In addition, the physiological ranges of motion of each vertebral level were based on the averages found by a study with cadaveric specimens (Ivancic *et al.* 2005). The intercept values necessary to calculate the injury criteria were obtained from the literature (Table 1).

Table 1: Intercept values for the calculation of the injury criteria.

Criterion	Intercept values	Injury threshold
NIC	-	NIC=10 (Pain threshold) (Li <i>et al.</i> 2019)
N_{km}	$F_{int} = 845 \text{ N}$ (Schmitt <i>et al.</i>)	$N_{km} = 1$ (Schmitt <i>et</i>

	2001) $M_{int} = 47.5 \text{ N m}/$ 81.1 N m (Schmitt <i>et al.</i> 2001) (extension/ flexion)	al. 2001)
--	--	-----------

RESULTS

Low-severity 4g impact simulations with the M50, M50_P and M50_{PC} head and neck models

All the obtained results were zeroed to the 0 ms time at the onset of the impact. The kinematics of the center of gravity (CoG) of the head were extracted from the rear impact simulations. The CoG X-displacement of the M50 and M50_P were within the corridors of one standard deviation of the experiments (Sato *et al.* 2014) (Figure 4). However, the M50_{PC} X-displacement was slightly higher than the corridors. The CoG Y-rotational displacement presented a similar trend to X-displacement initially. The M50 and M50_P models were inside of the experimental corridors up to the rebound phase at 170 ms, while the M50_{PC} were inside during rebound up to 220 ms. The contrasting M50_{PC} response to the other models was a result of the high forces generated by the small activation of the extensors during the stabilization phase of the model. Although this effect could be reduced by modifying the muscle activation parameters, for consistency with the previously published model, the activation parameters were kept constant throughout the study. The extensors are larger muscles, even a low activation was enough to increase the head rearward excursion in the M50_{PC} model (Figure 5). In addition, the developed M50_P and M50_{PC} models took 3 days to run on 32 CPUs, mainly due to the additional time required for the dynamic relaxation.

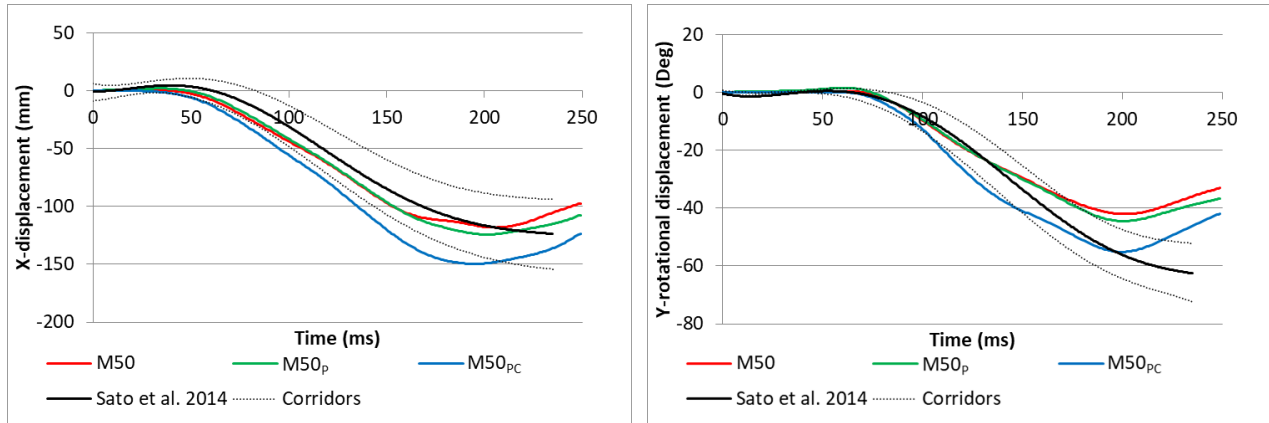


Figure 4: Kinematics of the head CoG for the 4g rear impact simulations. The X-displacement was calculated relative to T1. The corridors represent one standard deviation from the experimental average from Sato et al. (Sato et al. 2014).

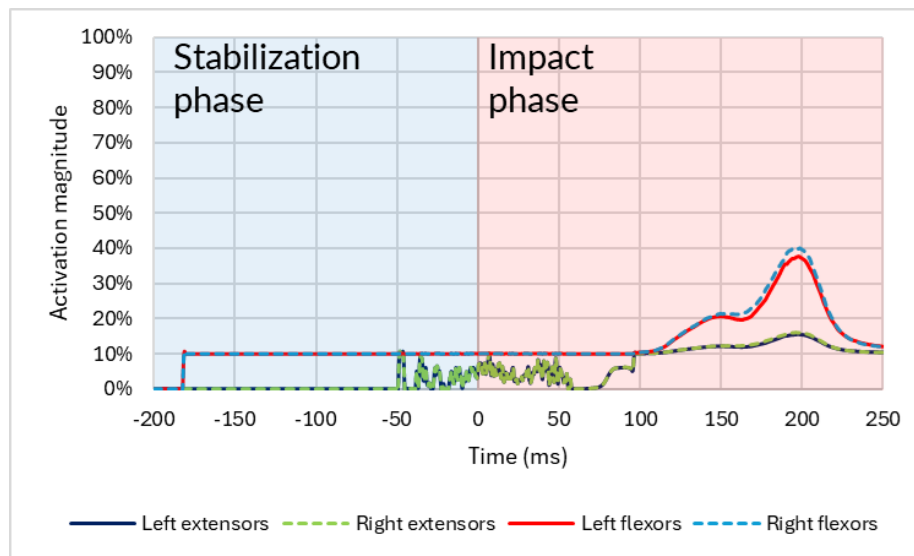


Figure 5: Muscle activation level for the M50PC in the 4g impact simulation. The muscles presented a baseline activation of around 10% before the impact. The timing of the muscle reflex activation was around 96 ms, inside the expected EMG values between 55 and 99 ms (Correia, McLachlin, and Cronin 2020). In addition, the activation magnitude of the extensors was lower than the flexors as expected. The flexors quickly deformed enough to achieve full CCR activation (10%) while the extensor oscillated around $t=0$. The oscillation was due to the neck achieving the final posture while the extensors presented some small variation on their stretch. The oscillation stopped after the impact reduced the deformation of the extensors.

The intervertebral rotations were extracted from the simulations, from C0 (skull) to C7 (Figure 6). The upper cervical flexion was more pronounced for the M50_{PC} during the S-shape phase and the neck extension was more pronounced during the C-shape

phase. The extension of the vertebra of the M50_{PC} was outside the corridors due to the activation of the extensors. Overall, the model joint kinematics followed trends evident in the experimental response.

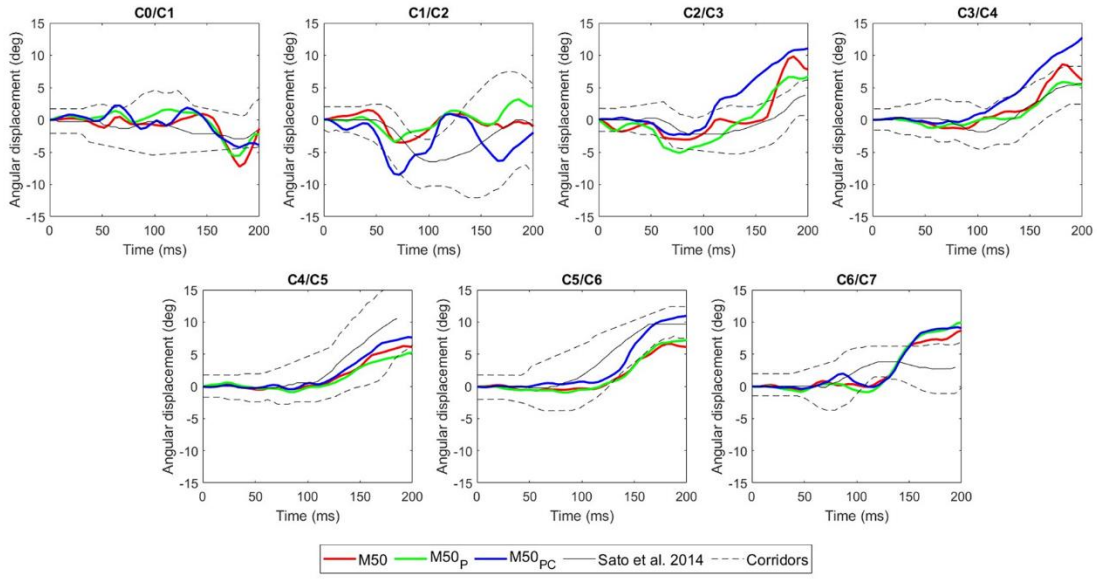


Figure 6: Intervertebral rotations from C0 (skull) to C7 for the three models. The corridors represent one standard deviation of the experimental data. The negative direction indicates flexion, and the positive direction indicates extension.

All three models presented similar trends concerning the injury criteria. The NIC (Figure 7) of all the models were below the pain threshold. The N_{km} (Figure 8) of the models were low during the S-shape phase (50 to 100 ms) but increased at the C-shape phase (above 100 ms). The IV-NIC (Figure 9) of the models also presented values higher than 1 during hyperextension of the C-shape phase. However, the

$M50_P$ crossed the value of IV-NIC=-1 at the C2-C3 joint during flexion. Overall, the model with pre-tension and without muscle activation obtained the lowest values for all injury criteria. In addition, the LNL was calculated for the models and indicated the same trends from the other injury criteria.

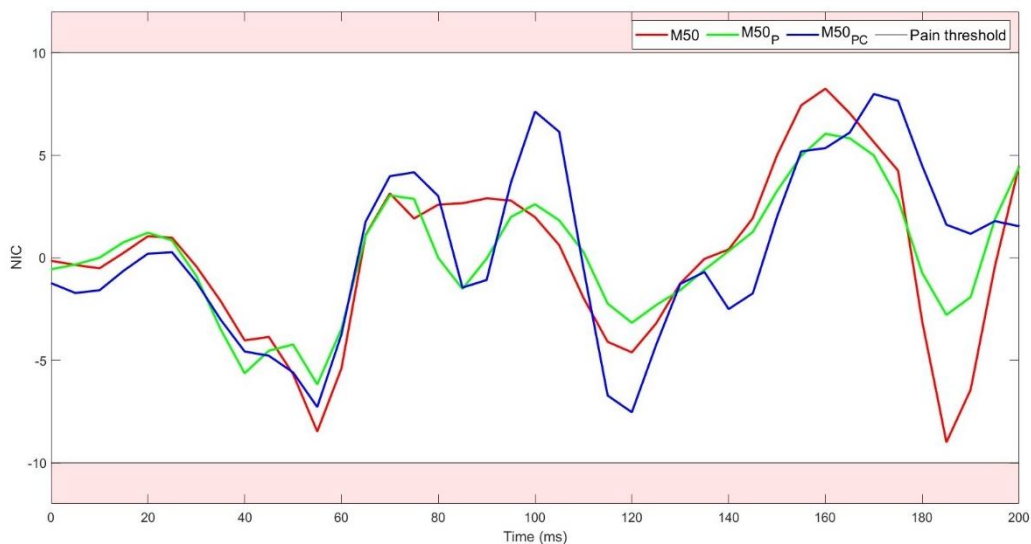


Figure 7: NIC values for the rear impact simulation for all three models were below the experimental pain threshold (NIC=10)

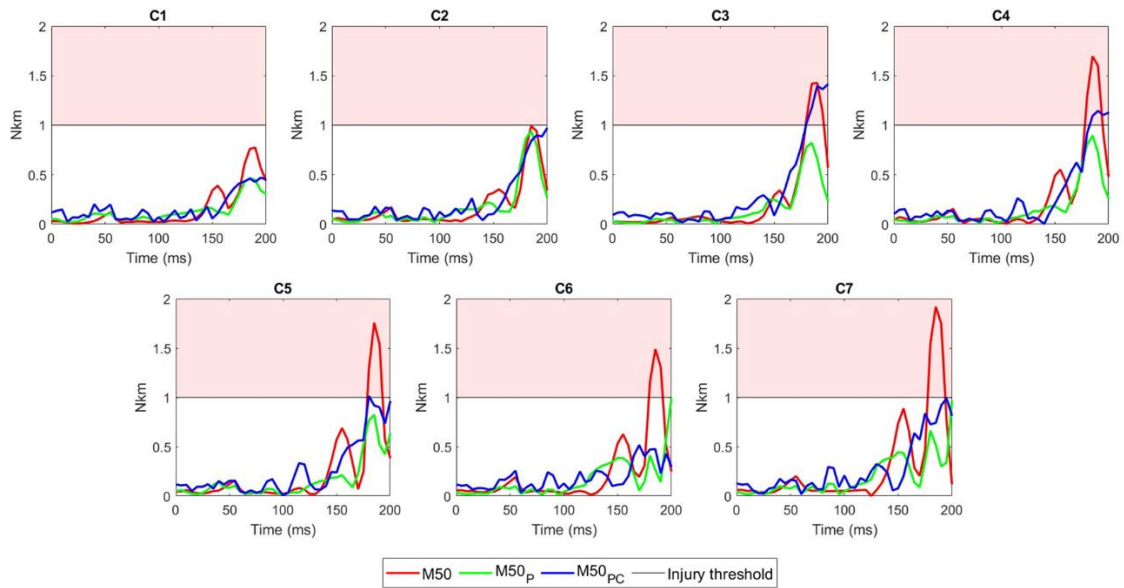


Figure 8: N_{km} values for the rear impact simulation for all three models. When calculating the N_{km} , the value of the M_{int} in flexion was used for the vertebral flexion and the M_{int} in extension was used for the vertebral extension.

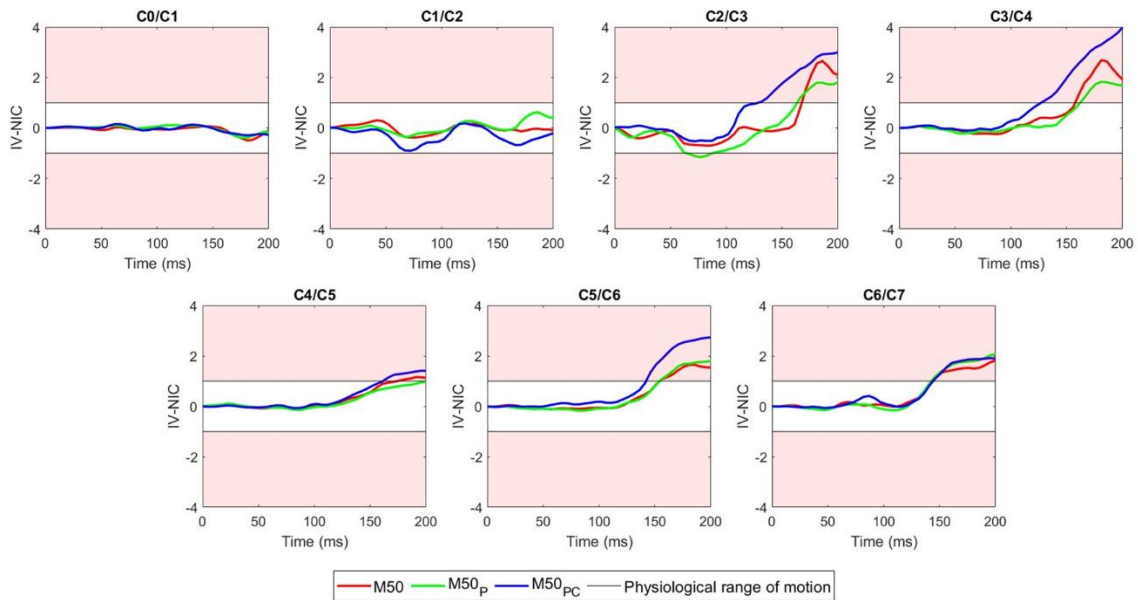


Figure 9: IV-NIC values for the rear impact simulation for all three models. When calculating the IV-NIC, the value of the physiological range of motion in flexion was used for the vertebral flexion (negative values) and the physiological range of motion in extension was used for the vertebral extension (positive values).

The distributions of strains in the muscles were different among the models (Figure 10). For example, the sternocleidomastoid MPS was higher than the

splenius capitis for the $M50_p$ model, while the opposite was true for the $M50$ and $M50_{PC}$. Also, the $M50_{PC}$ decreased the sternocleidomastoid MPS while

it increased the longus capitis MPS compared to the M50_p. Additionally, the average MPS increased with the addition of pre-tension and increased again with the addition of muscle activation. The average 95th percentile MPS were 0.12, 0.13, and 0.15 for the M50, M50_p, and M50_{PC}, respectively. The three muscles presenting the highest strains were all extensors: the rectus capitis lateralis (strains from 0.29 to 0.32), the trapezius (strains from 0.20 to 0.27) and the semispinalis cervicis (strains from 0.18 to 0.23).

High-severity 7g and 10g impact simulations with the M50_{PC} head and neck model

For the subsequent comparisons of increasing severity impacts, the intervertebral rotations were

also extracted from the simulations, from C0 (skull) to C7 (Figure 11). As expected, the 10g impact generated the highest intervertebral angular displacements in flexion and extension. However, the 7g impact presented slightly lower intervertebral angular rotations compared to the 4g impact. The 10g simulation provided useful data up to a simulation time of 175 ms and then terminated due to numerical instabilities in the tendon elements at the level of C1. Based on kinematic observation of the tendon elements, the model works without issues up to 175 ms after the impact. The large rotations of the vertebrae were a result of the impact severity.

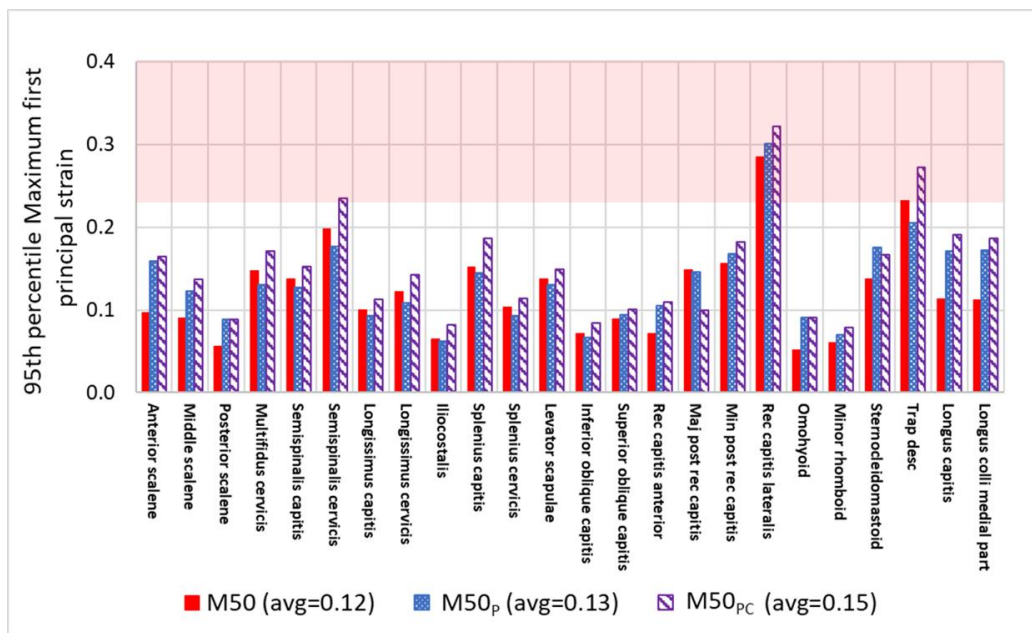


Figure 10: 95th percentile maximum first principal strain for each muscle in the 4g rear impact simulation for all three models. The average strains (avg) are shown inside parentheses. The red region shows values above the minimal injurious strain of 0.23.

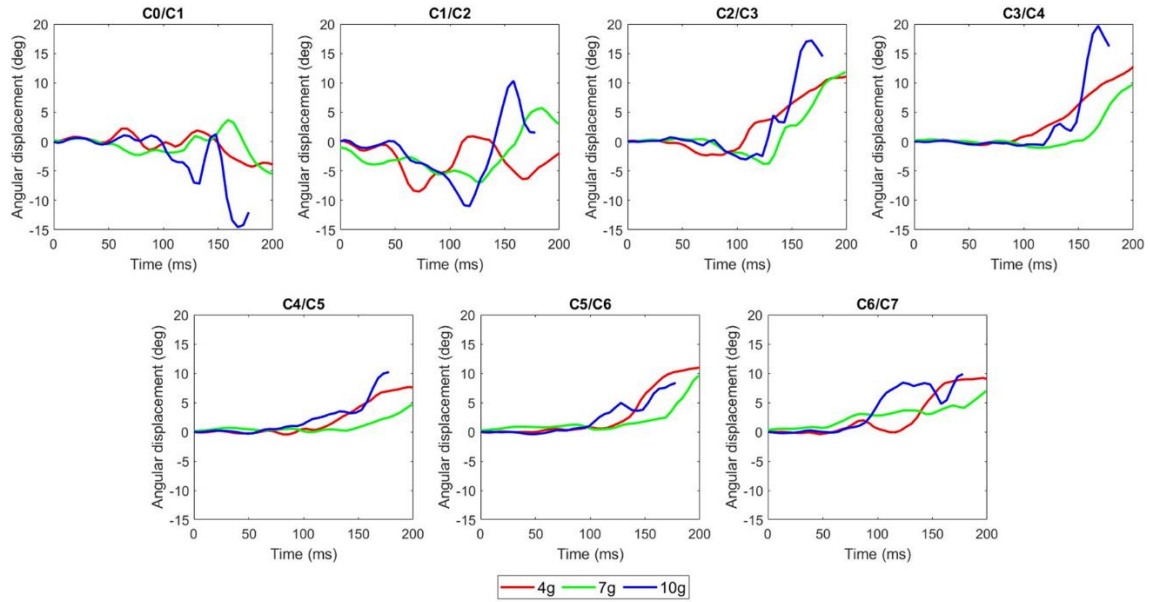


Figure 11: M50_{PC} intervertebral rotations from C0 (skull) to C7 for 4g, 7g, and 10g impact severities. The negative direction indicates flexion, and the positive direction indicates extension.

The calculated injury criteria values increased with impact severity except for the IV-NIC of the 7g case compared to the 4g case. The N_{km} (Figure 12) was low during the S-shape phase for all severities but increased at the C-shape phase. The IV-NIC (Figure

13) also presented values higher than 1 during hyperextension of the C-shape phase for all the severities. However, the 10g case crossed the value of IV-NIC=-1 at the C1-C2 joint during flexion.

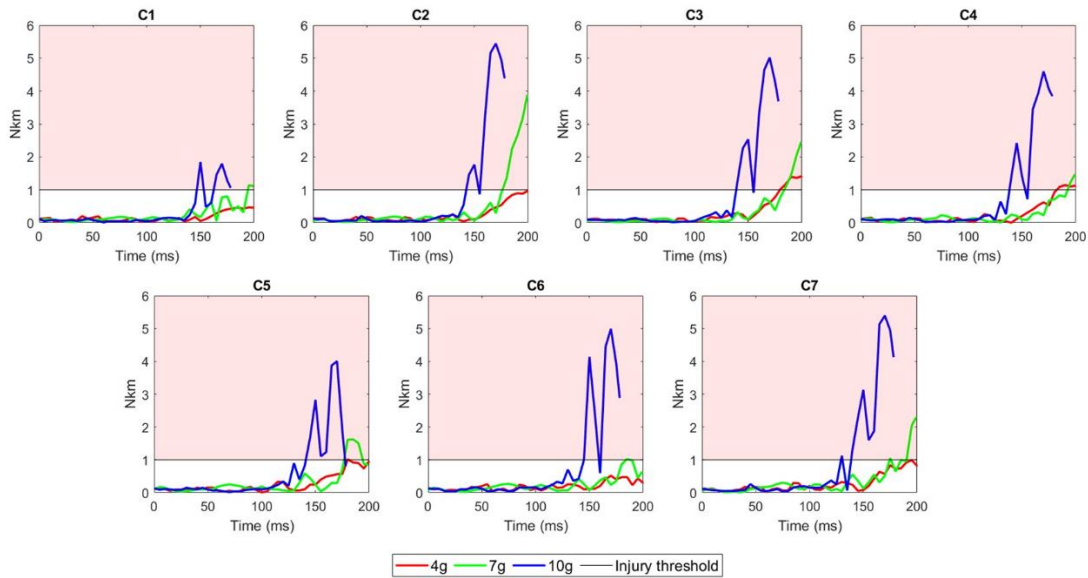


Figure 12: M50_{PC} N_{km} values for the 4g, 7g, and 10g rear impact simulations. When calculating the N_{km} , the value of the M_{int} in flexion was used for the vertebral flexion and the M_{int} in extension was used for the vertebral extension.

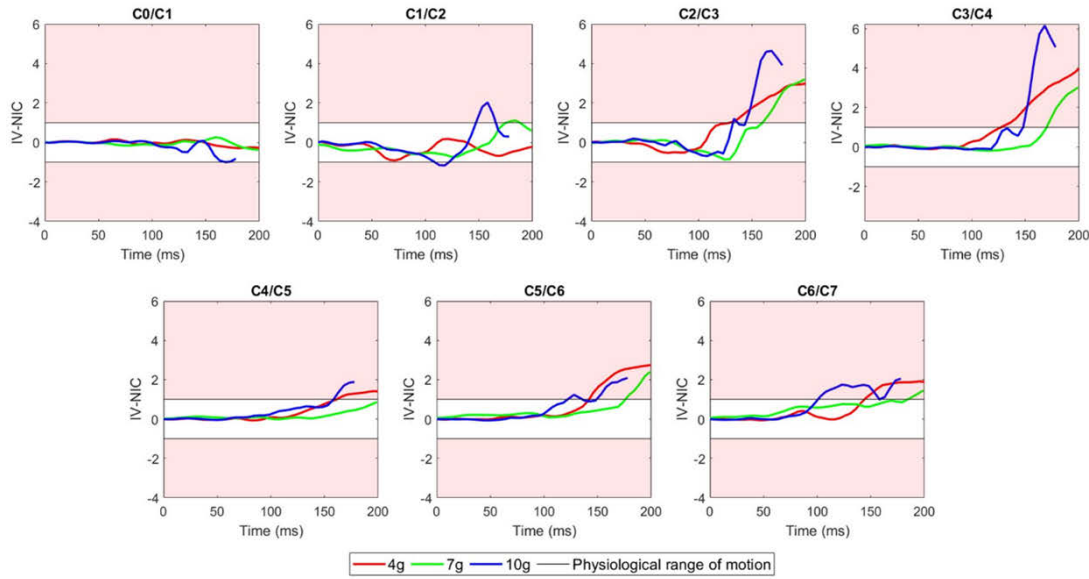


Figure 13: M50_{PC} IV-NIC values for the 4g, 7g, and 10g rear impact simulations. When calculating the IV-NIC, the value of the physiological range of motion in flexion was used for the vertebral flexion (negative values) and the physiological range of motion in extension was used for the vertebral extension (positive values).

The highest average muscle strain (0.22) was found in the 10g impact while the 4g and 7g cases had the same average strain (0.15) (Figure 14). For all the severities, the three extensors presenting the highest strains were: the rectus capitis lateralis (strains from 0.25 to 0.44), the trapezius (strains from 0.27 to

0.41), and the semispinalis cervicis (strains from 0.21 to 0.33). However, for the 10g impact, a flexor, the rectus capitis lateralis, also presented a high strain (0.43) in contrast to the lower severities (0.11 to 0.15) in which only the extensors presented the highest strains.

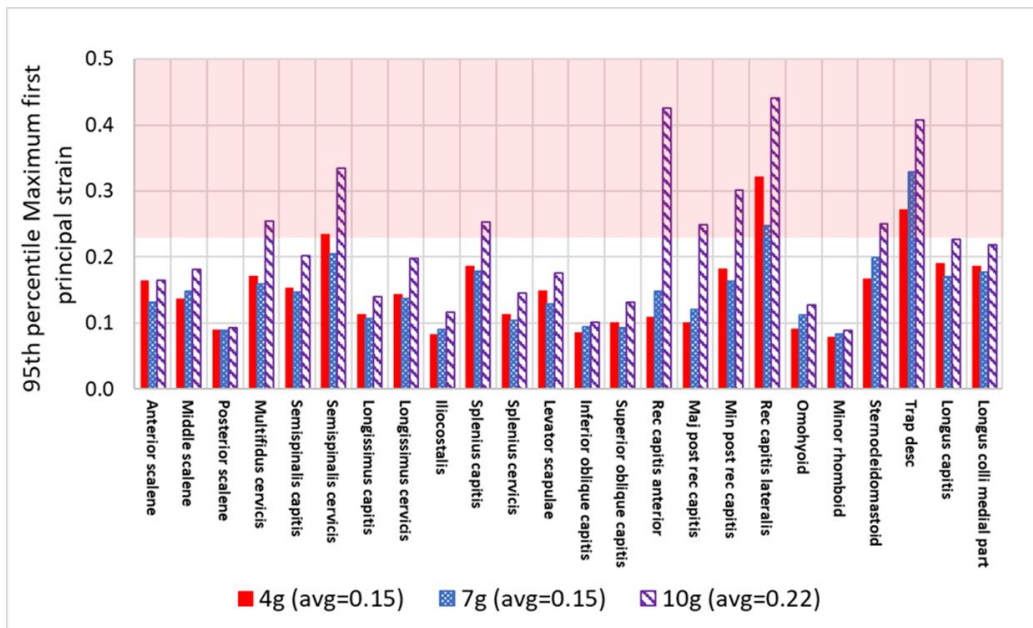


Figure 14: 95th percentile maximum first principal strain for each muscle in the M50_{PC} for the 4g, 7g, and 10g rear impact simulations. The average strains (avg) are shown inside parentheses. The red region shows values above the minimal injurious strain of 0.23.

DISCUSSION

The integration of the muscle pre-tension and a closed-loop muscle activation controller was successfully implemented in the GHBMC head and neck model, resulting in head and vertebral kinematics from the model that were within or close to the response corridors of the human volunteers for a 4g impact. The M50_{PC} obtained slightly higher head displacements and rotations, which is expected due to the additional force produced by the muscles, especially the larger extensors.

Compared to the M50, the M50_P increased the upper cervical spine flexion from 7.5° degrees to 8.9° degrees, and the M50_{PC} increased it to 11.1°. Both M50_P and M50_{PC} approximated peak C1-C4 flexion to the experimental average of 10.3° degrees as expected for a better representation of the muscle forces. Nevertheless, the additional loads of the muscle activation of the M50_{PC} were required to achieve C1-C2 peak flexion similar to the experiments. However, the M50_{PC} resulted in a higher extension at the C2-C3 level during the C-shape phase, indicating a tradeoff between these two phases in the current model. The simulated vertebral joints presented negligible shear (Appendix Figure A2 and A3) compared to the experiments from Sato et al. (Sato et al. 2014). The low shear possibly indicates differences in the intervertebral disk implementation and bony geometry that may have led to the trade-offs observed in the model.

The distributions of the muscle strains were different among models (Figure 10) even though the differences in head kinematics were small. This contrast shows that obtaining precise values for usually neglected aspects of the muscles such as pre-tension is essential to quantify soft tissue injurious strains in low severity impacts. The highest values of MPS in all models were in the trapezius, rectus capitis lateralis, and semispinalis cervicis. These three muscles are extensors. For the M50, the trapezius and rectus capitis lateralis MPS surpassed the lowest strain in which injury was identified in the literature (0.23) (Hasselmann et al. 1995). For the M50_P, only the rectus capitis lateralis surpassed the lowest strain in which injury was identified in the literature. For the M50_{PC}, the trapezius, rectus capitis lateralis and semispinalis cervicis MPS surpassed the lowest strain in which injury was identified in the literature. The muscle strains indicated a potential risk of injury in the posterior region of the lower cervical spine and at the posterior region near the base of the skull. The injury regions identified agreed with MRI studies (Elliott et al. 2006; Lund et al. 2023; Snodgrass et al. 2022) of whiplash patients that

identified a higher increase of fatty tissue (a signal of injury) at the semispinalis cervicis, multifidus, trapezius, and rectus capitis posterior major and minor (both in close proximity to the rectus capitis lateralis) after the impact. The possibility of injury also agreed with the reported pain felt by the volunteers during the sled tests (Sato et al. 2014) used for the boundary conditions of the simulations.

Importantly, even with the higher flexion of the M50_{PC} the IV-NIC, and N_{km} indicated a higher risk of injury during the C-shape phase. The trend indicated by these injury criteria was in agreement with the timing of higher strains in the muscles. However, the pain threshold was not crossed by any of the models for the NIC, indicating that this metric may be insensitive to such low-severity impacts. The IV-NIC showed potential injury from C2 to C7 for all models. The N_{km} showed potential injury in all vertebral levels for the M50, no potential injury for the M50_P, and only potential injury from C2 to C4 for the M50_{PC}. The reduced sensitivity of the IV-NIC compared to N_{km} to the different models is expected due to the smaller changes in vertebral displacement compared to the larger changes in load distribution. For the IV-NIC, the C2-C3 values for the M50_P were slightly beyond the injury threshold, which may indicate that for higher severities of similar impacts, the S-shape may become increasingly injurious. This data also agrees with experimental data that indicated injury at C2-C3 and C5-C6 levels, showing the importance of muscle pre-tension to the injury analysis at low-severity impacts. Nevertheless, the hyperextension phase still presented higher values of the injury criteria, which is in agreement with the analysis of tissues strains during neck extension conducted in the rectus capitis posterior minor (Hallgren and Rowan 2021). Overall, the pre-tension reduced the injury criteria values even though it increased average muscle strains, indicating that the investigated injury criteria may not be adequate for understanding the soft tissue response. The ligaments, vertebrae and discs did not present injurious loads in any of the simulations, which was also in contrast to what was identified by the injury criteria. In addition, a new injury criterion relating force and activation of 1D Hill-type elements to muscle injury was proposed by Nölle *et al.* (Nölle et al. 2022), and could be adapted to the GHBMC model in the future to further investigate the muscle injury possibility.

The overall analysis of the increase in impact severity indicated that the vertebral angular displacements and calculated injury criteria were highest for the 10g case as expected. The 4g and 7g presented

comparable values for the intervertebral kinematics, but not for the N_{km} . One possible explanation is the vertebral kinematics being maintained between these two severities may be due to muscle activation, which would explain the increase in loads for the 7g case. This would agree with previous studies (Liang et al. 2022) that indicated that muscle activation could help protect the neck against injury. Another possible explanation is the use in the simulations of boundary conditions from two different studies for the different severities; therefore, the 7g response of the model may not follow a progressive increase compared to the 4g pulse. However, the 7g and 10g cases were from the same study and therefore presented the expected increase in vertebral kinematics with severity. The distribution of muscle strain also increased for the 10g impact with the extensors displaying the highest strain. In contrast, the M50_{PC} had one flexor, rectus capitis anterior, presenting one of the highest strains. This flexor is a small muscle at the base of the skull which explains the large deformations only when the muscle was actively contracted. The 10g impact IV-NIC also surpassed the physiological range of motion during the S-shape in opposition to the 4g or 7g cases. The high severity needed to onset the possibility of injury during the S-shape phase agrees with the literature that uses this mechanism to justify males being less prone to whiplash injury than females due to anthropometric differences (John et al. 2019; Stemper, Yoganandan, and Pintar 2003). The 10g simulation terminated prematurely due to numerical instability in a tendon element connected to a muscle beam element. The small beam elements for the active muscle presented extremely high relative stretches near the tendons in the 10g impact severity generating instabilities during the Hill-type element muscle force calculation. The simulation could be run to completion if longer elements were implemented in the future.

The current study includes some limitations. The scarcity of *in vivo* force and strain data for muscle tissue and vertebral kinematics during rear impacts makes further validation of the simulated results challenging. Recent ultrasound studies (Budzikowski and Murray 2023; Zheng et al. 2021) were able to measure volumetric changes in large muscles during voluntary contraction and may be adapted to help validate the simulated deformations during impacts. For comparison with the IV-NIC, the N_{km} was used to observe the loads in all vertebral joints although it was developed for measuring loads at the occiput. It was assumed the N_{km} intercepts of all vertebral levels were the same as the ones of the occiput. However, obtaining N_{km} intercepts for each vertebral joint

would be ideal. The simplified grouping of the muscles into flexors and extensors may not capture all the complexities of pre-tension and activation of individual muscles. The sternohyoid and sternothyroid-thyrohyoid muscles were not considered in the strain analysis as they reported high localized strains in the T1 region, especially for the M50_{PC}. The localized high strains were deemed artifacts due to the muscles, adipose tissue and skin being fixed to T1 for the extracted head and neck model. In addition, the M50_{PC} model generated a higher head extension than the experiments, indicating the need to further adapt the closed-loop controller for a model with pre-tension. One parameter that could be modified would be the cocontraction ratio between flexors and extensors that were not updated for the model with pre-tension. Comments about the results should be reserved for the Discussion section, where all the study findings can be discussed and integrated with the results in the literature. The Discussion section should summarize what was done and what was found, while simultaneously providing commentary to interpret the results. Any limitations of the findings, or possible sources and magnitudes of error, should be mentioned. The Discussion section is also where the authors will recommend or indicate plans for future research.

CONCLUSIONS

The current study was the first to analyze the effect of muscle pre-tension and muscle activation on head and vertebral kinematics, and the possibility of injury, using the M50 head and neck model.

The more pronounced upper cervical S-shape of the M50_{PC} better represented the experimental peak flexion but had a more pronounced C-shape and head kinematics than the tests with volunteers.

The muscle strain increased progressively with the inclusion of pre-tension and muscle activation. The distribution of muscle strains among the muscles varied for the three models. The M50_{PC} strains indicated the possibility of injury in muscles that better represented the regions of pain from experiments. Furthermore, only the model with muscle activation showed possible muscle injury in the deep muscles (semispinalis cervicis) as expected from the literature. In addition, the strains increased with impact severity as expected.

The predicted maximum muscle strains, and injury metrics in all but one model configuration identified that the C-shape was the main injurious phase for the impact severities investigated. Only the M50_{PC}

indicated injury for the IV-NIC criterium at the C2-C3 level during the S-shape, as was previously suggested in the literature. It is important to note that the current study focused on the muscle response although other tissues such as the facet joints were raised as potential regions of WAD injury.

The current study was the first to analyze the relationship between muscle strain during rear impacts and neck injury criteria. Although further experiments are still needed to validate the current study results, the proposed models can help inform regions of interest for injury analysis and are a step toward improving understanding of soft-tissue injury mechanisms.

ACKNOWLEDGMENTS

The authors would like to acknowledge the financial support for this research provided by the Natural Sciences and Engineering Research Council of Canada. This research was undertaken, in part, thanks to funding from the Canada Research Chairs Program. The head-and-neck model was provided by the Global Human Body Models Consortium. Computing resources were provided by the Digital Research Alliance of Canada.

REFERENCES

- Best, T. M., J. H. McElhaney, W. E. Garrett, and B. S. Myers. 1995. "Axial Strain Measurements in Skeletal Muscle at Various Strain Rates." *Journal of Biomechanical Engineering* 117(3):262–65. doi: 10.1115/1.2794179.
- Brault, John R., Gunter P. Siegmund, and Jeffrey B. Wheeler. 2000. "Cervical Muscle Response during Whiplash: Evidence of a Lengthening Muscle Contraction." *Clinical Biomechanics* 15(6):426–35. doi: 10.1016/S0268-0033(99)00097-2.
- Budzikowski, Jorie D., and Wendy M. Murray. 2023. "Multi-Sweep 3-Dimensional Ultrasound Is Accurate for in Vivo Muscle Volume Quantification, Expanding Use to Larger Muscles." *Journal of Biomechanics* 151:111501. doi: 10.1016/j.jbiomech.2023.111501.
- Bumberger, Roman, Memis Acar, and Kaddour Bouazza-Marouf. 2020. "Importance of Intervertebral Displacement for Whiplash Investigations." *International Journal of Crashworthiness* 25(4):376–90. doi: 10.1080/13588265.2019.1594548.

- Corrales, Miguel A., and D. S. Cronin. 2021. "Sex, Age and Stature Affects Neck Biomechanical Responses in Frontal and Rear Impacts Assessed Using Finite Element Head and Neck Models." *Frontiers in Bioengineering and Biotechnology* 9:681134. doi: 10.3389/fbioe.2021.681134.
- Corrales, Miguel, Matheus Correia, and Duane Cronin. 2021. "Active and Passive Musculature Coupling Strategy to Improve Muscle Strain Prediction." Unpublished.
- Correia, Matheus A., Miguel A. Corrales, Stewart D. McLachlin, and Duane S. Cronin. 2023. "Effect of Muscle Pre-tension and Pre-impact Neck Posture on the Kinematic Response of the Cervical Spine in Simulated Low-speed Rear Impacts." *International Journal for Numerical Methods in Biomedical Engineering* 39(11):e3761. doi: 10.1002/cnm.3761.
- Correia, Matheus A., Stewart D. McLachlin, and Duane S. Cronin. 2020. "Optimization of Muscle Activation Schemes in a Finite Element Neck Model Simulating Volunteer Frontal Impact Scenarios." *Journal of Biomechanics* 104:109754. doi: 10.1016/j.jbiomech.2020.109754.
- Correia, Matheus A., Stewart D. McLachlin, and Duane S. Cronin. 2021. "Vestibulocollic and Cervicocollic Muscle Reflexes in a Finite Element Neck Model During Multidirectional Impacts." *Annals of Biomedical Engineering* 49(7):1645–56. doi: 10.1007/s10439-021-02783-2.
- Deng, Bing, Paul C. Begeman, King H. Yang, Scott Tashman, and Albert I. King. 2000. "Kinematics of Human Cadaver Cervical Spine During Low Speed Rear-End Impacts." Pp. 2000-01-SC13 in.
- DeWit, Jennifer A., and Duane S. Cronin. 2012. "Cervical Spine Segment Finite Element Model for Traumatic Injury Prediction." *Journal of the Mechanical Behavior of Biomedical Materials* 10:138–50. doi: 10.1016/j.jmbbm.2012.02.015.
- Elliott, James, Gwendolen Jull, Jon Timothy Noteboom, Ross Darnell, Graham Galloway, and Wayne W. Gibbon. 2006. "Fatty Infiltration in the Cervical Extensor Muscles in Persistent Whiplash-Associated Disorders: A Magnetic Resonance Imaging Analysis." *Spine* 31(22):E847–55. doi: 10.1097/01.brs.0000240841.07050.34.
- Gierczycka, Donata, Aleksander Rycman, and Duane Cronin. 2021. "Importance of Passive Muscle,

- Skin, and Adipose Tissue Mechanical Properties on Head and Neck Response in Rear Impacts Assessed with a Finite Element Model.” *Traffic Injury Prevention* 22(5):407–12. doi: 10.1080/15389588.2021.1918685.
- Hadagali, Prasannaah, and Duane S. Cronin. 2023. “Enhancing the Biofidelity of an Upper Cervical Spine Finite Element Model Within the Physiologic Range of Motion and Its Effect on the Full Ligamentous Neck Model Response.” *Journal of Biomechanical Engineering* 145(1):011007. doi: 10.1115/1.4055037.
- Hallgren, Richard C., and Jacob J. Rowan. 2021. “Assessment of Potential Strain Injury to Rectus Capitis Posterior Minor Muscles during Whiplash Type Distortions of the Cervical Spine.” *Journal of Osteopathic Medicine* 121(9):747–53. doi: 10.1515/jom-2021-0094.
- Happee, Riender, Edo De Bruijn, Patrick A. Forbes, and Frans C. T. Van Der Helm. 2017. “Dynamic Head-Neck Stabilization and Modulation with Perturbation Bandwidth Investigated Using a Multisegment Neuromuscular Model.” *Journal of Biomechanics* 58:203–11. doi: 10.1016/j.jbiomech.2017.05.005.
- Hasselmann, Carl T., Thomas M. Best, Anthony V. Seaber, and William E. Garrett. 1995. “A Threshold and Continuum of Injury During Active Stretch of Rabbit Skeletal Muscle.” *The American Journal of Sports Medicine* 23(1):65–73. doi: 10.1177/036354659502300111.
- Hayashi, Kazuhiro, Kenji Miki, Tatsunori Ikemoto, Takahiro Ushida, Yukiko Shiro, Tomoko Tetsunaga, Toshifumi Takasusuki, Masako Hosoi, and Masao Yukioka. 2023. “Predictors of High-Cost Patients with Acute Whiplash-Associated Disorder in Japan” edited by A. M. Mosa. *PLOS ONE* 18(6):e0287676. doi: 10.1371/journal.pone.0287676.
- Ivancic, Paul C., Shigeki Ito, Manohar M. Panjabi, Adam M. Pearson, Yasuhiro Tominaga, Jaw-Lin Wang, and S. Elena Gimenez. 2005. “Intervertebral Neck Injury Criterion for Simulated Frontal Impacts.” *Traffic Injury Prevention* 6(2):175–84. doi: 10.1080/15389580590931671.
- Jagodnik, Kathleen M., Dimitra Blana, Antonie J. Van Den Bogert, and Robert F. Kirsch. 2015. “An Optimized Proportional-Derivative Controller for the Human Upper Extremity with Gravity.” *Journal of Biomechanics* 48(13):3692–3700. doi: 10.1016/j.jbiomech.2015.08.016.
- John, Jobin D., Gurunathan Saravana Kumar, and Narayan Yoganandan. 2019. “Rear-Impact Neck Whiplash: Role of Head Inertial Properties and Spine Morphological Variations on Segmental Rotations.” *Journal of Biomechanical Engineering* 141(11):111008. doi: 10.1115/1.4043666.
- Johnson, Dale, Bharath Koya, and F. Scott Gayzik. 2020. “Comparison of Neck Injury Criteria Values Across Human Body Models of Varying Complexity.” *Frontiers in Bioengineering and Biotechnology* 8:985. doi: 10.3389/fbioe.2020.00985.
- Li, Fan, Nian-song Liu, Hong-geng Li, Biao Zhang, Shi-wei Tian, Ming-gang Tan, and Baptiste Sandoz. 2019. “A Review of Neck Injury and Protection in Vehicle Accidents.” *Transportation Safety and Environment* 1(2):89–105. doi: 10.1093/tse/tdz012.
- Liang, Ziyang, Fuhao Mo, Zhefen Zheng, Yuandong Li, Ye Tian, Xiaobing Jiang, and Tang Liu. 2022. “Quantitative Cervical Spine Injury Responses in Whiplash Loading with a Numerical Method of Natural Neural Reflex Consideration.” *Computer Methods and Programs in Biomedicine* 219:106761. doi: 10.1016/j.cmpb.2022.106761.
- Lund, Nils, Olof Dahlqvist Leinhard, James M. Elliott, Gunnel Peterson, Magnus Borga, Peter Zsigmond, Anette Karlsson, and Anneli Peolsson. 2023. “Fatty Infiltrate and Neck Muscle Volume in Individuals with Chronic Whiplash Associated Disorders Compared to Healthy Controls – a Cross Sectional Case–Control Study.” *BMC Musculoskeletal Disorders* 24(1):181. doi: 10.1186/s12891-023-06289-x.
- Morrow, Duane A., Tammy L. Haut Donahue, Gregory M. Odegard, and Kenton R. Kaufman. 2010. “Transversely Isotropic Tensile Material Properties of Skeletal Muscle Tissue.” *Journal of the Mechanical Behavior of Biomedical Materials* 3(1):124–29. doi: 10.1016/j.jmbbm.2009.03.004.
- Nölle, Lennart V., Atul Mishra, Oleksandr V. Martynenko, and Syn Schmitt. 2022. “Evaluation of Muscle Strain Injury Severity in Active Human Body Models.” *Journal of the Mechanical Behavior of Biomedical Materials* 135:105463. doi: 10.1016/j.jmbbm.2022.105463.

- Putra, I. Putu A., Johan Iraeus, Fusako Sato, Mats Y. Svensson, Astrid Linder, and Robert Thomson. 2021. "Optimization of Female Head-Neck Model with Active Reflexive Cervical Muscles in Low Severity Rear Impact Collisions." *Annals of Biomedical Engineering* 49(1):115–28. doi: 10.1007/s10439-020-02512-1.
- Putra, I. Putu A., and Robert Thomson. 2022. "Analysis of Control Strategies for VIVA OpenHBM with Active Reflexive Neck Muscles." *Biomechanics and Modeling in Mechanobiology* 21(6):1731–42. doi: 10.1007/s10237-022-01616-y.
- Sato, F., M. Odani, Y. Miyazaki, T. Nakajima, J. A. Makoshi, K. Yamazaki, K. Ono, M. Svensson, J. Osth, S. Morikawa, S. Schick, and A. Ferreira Perez. 2016. "Investigation of Whole Spine Alignment Patterns in Automotive Seated Posture Using Upright Open MRI Systems."
- Sato, Fusako, Taichi Nakajima, Koshiro Ono, Mats Svensson, Karin Brolin, and Koji Kaneoka. 2014. "Dynamic Cervical Vertebral Motion of Female and Male Volunteers and Analysis of Its Interaction with Head/Neck/Torso Behavior during Low-Speed Rear Impact."
- Schmitt, Kai-Uwe, Markus Muser, Peter Niederer, and Felix Walz. 2001. "A New Neck Injury Criterion Candidate For Rear-End Collisions Taking Into Account Shear Forces And Bending Moments."
- Schmitt, Kai-Uwe, Peter F. Niederer, Duane S. Cronin, Markus H. Muser, and Felix Walz. 2014. *Trauma Biomechanics: An Introduction to Injury Biomechanics*. Berlin, Heidelberg: Springer Berlin Heidelberg.
- Snodgrass, Suzanne J., Peter Stanwell, Kenneth A. Weber, Samala Shepherd, Olivia Kennedy, Hannah J. Thompson, and James M. Elliott. 2022. "Greater Muscle Volume and Muscle Fat Infiltrate in the Deep Cervical Spine Extensor Muscles (Multifidus with Semispinalis Cervicis) in Individuals with Chronic Idiopathic Neck Pain Compared to Age and Sex-Matched Asymptomatic Controls: A Cross-Sectional Study." *BMC Musculoskeletal Disorders* 23(1):973. doi: 10.1186/s12891-022-05924-3.
- Stemper, Brian D., and Brian D. Corner. 2016. "Whiplash-Associated Disorders: Occupant Kinematics and Neck Morphology." *Journal of Orthopaedic & Sports Physical Therapy* 46(10):834–44. doi: 10.2519/jospt.2016.6846.
- Stemper, Brian D., Narayan Yoganandan, and Frank A. Pintar. 2003. "Gender Dependent Cervical Spine Segmental Kinematics during Whiplash." *Journal of Biomechanics* 36(9):1281–89. doi: 10.1016/S0021-9290(03)00159-3.
- Stemper, Brian D., Narayan Yoganandan, and Frank A. Pintar. 2004. "Response Corridors of the Human Head-Neck Complex in Rear Impact." *Annual Proceedings – Association for the Advancement of Automotive Medicine* 48:149–63.
- Swain, Ritwik, and Grégoire S. Larue. 2024. "Looking Back in the Rearview: Insights into Queensland's Rear-End Crashes." *Traffic Injury Prevention* 25(2):138–46. doi: 10.1080/15389588.2023.2267710.
- Vasavada, Anita N., John R. Brault, and Gunter P. Siegmund. 2007. "Musculotendon and Fascicle Strains in Anterior and Posterior Neck Muscles During Whiplash Injury." *Spine* 32(7):756–65. doi: 10.1097/01.brs.0000259058.00460.69.
- Wakeling, James M., Míriam Febrer-Nafria, and Friedl De Groote. 2023. "A Review of the Efforts to Develop Muscle and Musculoskeletal Models for Biomechanics in the Last 50 Years." *Journal of Biomechanics* 155:111657. doi: 10.1016/j.jbiomech.2023.111657.
- Yoganandan, Narayan, Balaji Harinathan, and Aditya Vedantam. 2024. "Cervical Column and Cord and Column Responses in Whiplash With Stenosis: A Finite Element Modeling Study." *Journal of Engineering and Science in Medical Diagnostics and Therapy* 7(2):021003. doi: 10.1115/1.4063250.
- Zheng, Yang, Henry Shin, Derek G. Kamper, and Xiaogang Hu. 2021. "Automatic Detection of Contracting Muscle Regions via the Deformation Field of Transverse Ultrasound Images: A Feasibility Study." *Annals of Biomedical Engineering* 49(1):354–66. doi: 10.1007/s10439-020-02557-2.

APPENDIX

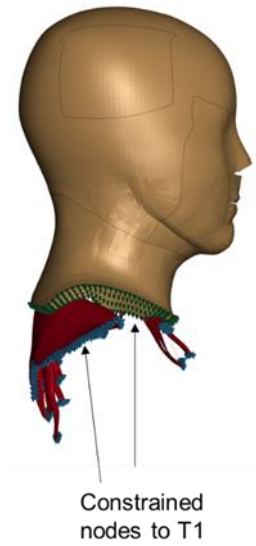


Figure A1: Muscle, skin, and flesh nodes rigidly constrained to T1.

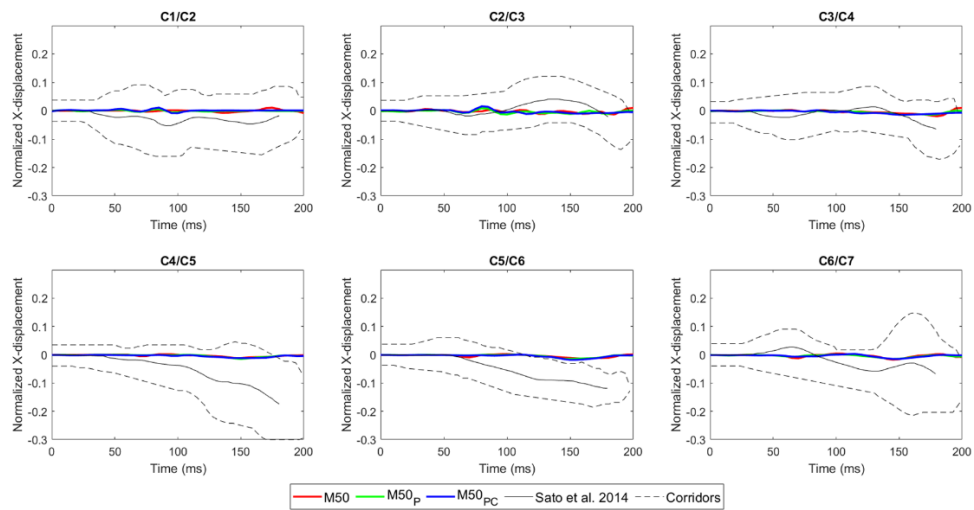


Figure A2: Intervertebral X-displacement from C0 (skull) to C7 for the three models. The corridors represent one standard deviation of the experimental data.

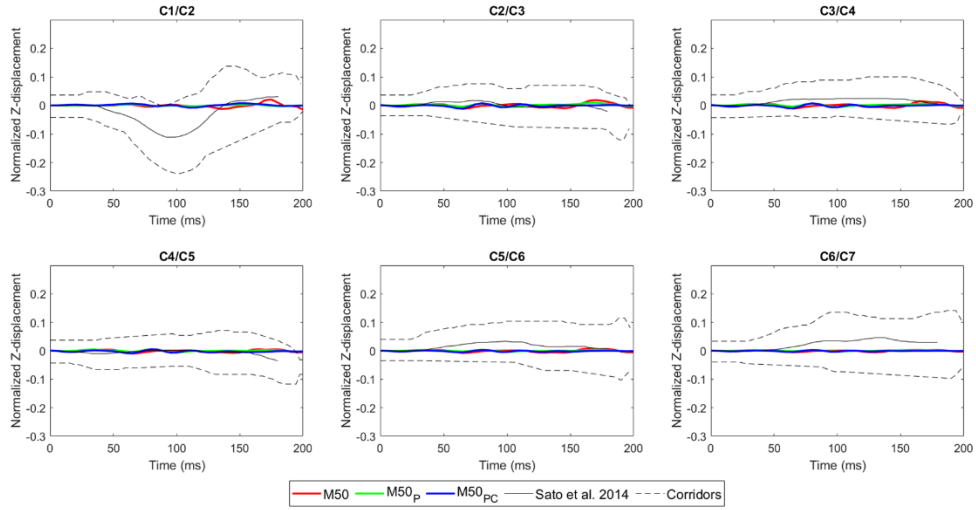


Figure A3: Intervertebral Z-displacement from C0 (skull) to C7 for the three models. The corridors represent one standard deviation of the experimental data.

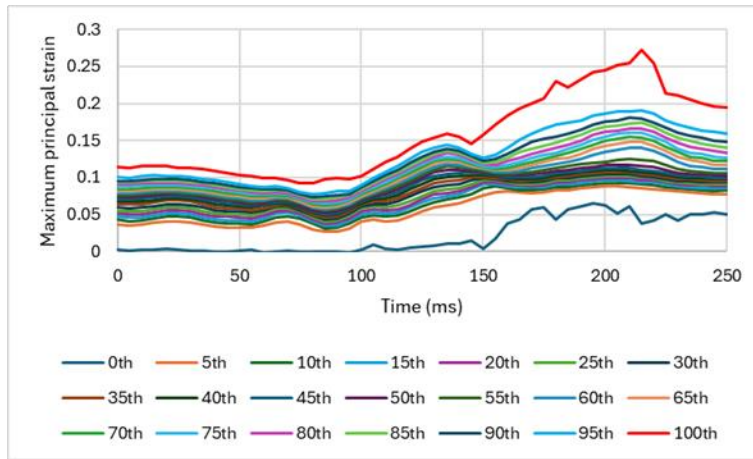


Figure A4: The MPS of the longus capitis are shown for the M50PC in the 4g impact for all percentiles. The 95th percentile included strains in the main portion of the muscle, while the 100th percentile strain corresponded to the muscle-tendon attachment.

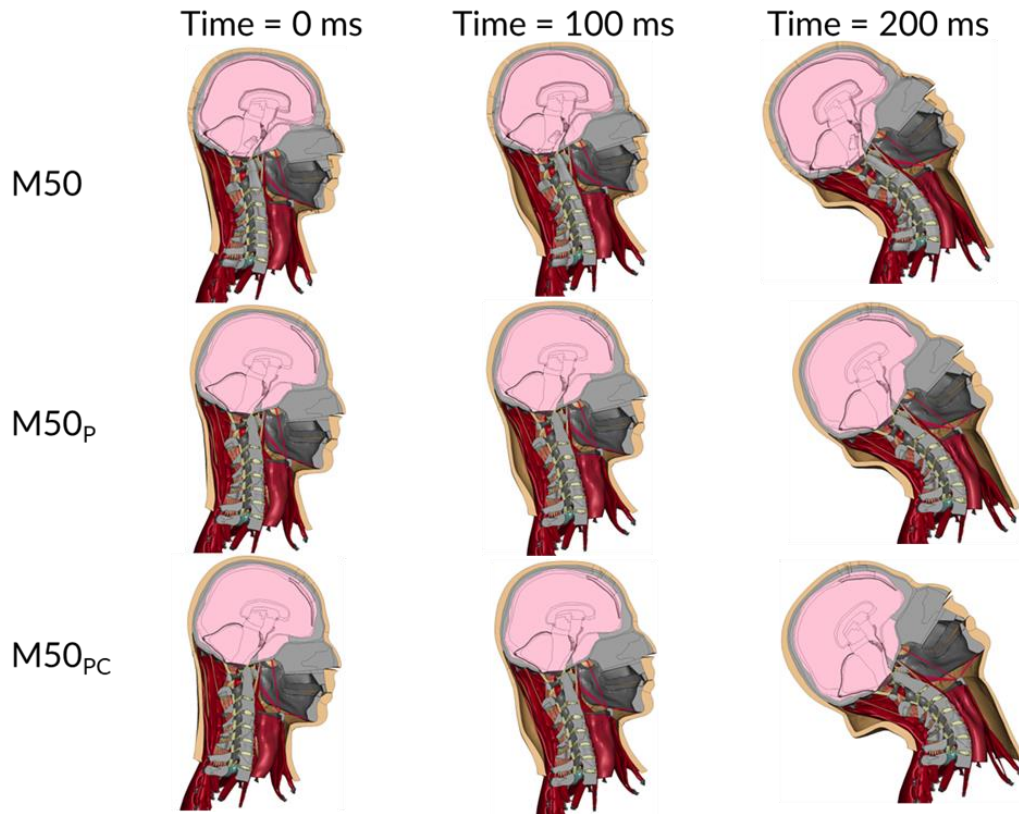


Figure A5: Cross-section of the M50, M50P, and M50PC models in the 4g rear impacts at 0 ms, 100 ms, and 200 ms. The red rectangle shows the higher M50P and M50PC upper cervical flexion during the S-shape phase compared to the M50.